

# Stable laser-driven proton beam acceleration from a two-specie ultra-thin foil

T. P. Yu,<sup>1,2</sup> A. Pukhov,<sup>1,\*</sup> G. Shvets,<sup>3,4</sup> and M. Chen<sup>5</sup>

<sup>1</sup>*Institut für Theoretische Physik I,  
Heinrich-Heine-Universität Düsseldorf, 40225 Düsseldorf, Germany*

<sup>2</sup>*Department of Physics, National University of  
Defense Technology, Changsha 410073, China*

<sup>3</sup>*Univ Texas Austin, Dept Phys, Austin, TX 78712 USA*

<sup>4</sup>*Univ Texas Austin, Inst Fus Studies, Austin, TX 78712 USA*

<sup>5</sup>*Accelerator & Fusion Research Division,  
Lawrence Berkeley National Laboratory, Berkeley, California 94720, USA*

(Dated: July 14, 2021)

## Abstract

By using multi-dimensional particle-in-cell simulation, we present a new regime of stable proton beam acceleration which takes place when a two-specie shaped foil is illuminated by a circularly polarized laser pulse. It is observed that the lighter protons are nearly-instantaneously separated from the heavier carbon ions due to the charge-to-mass ratio difference. The heavy-ions layer extensively expands in space and acts to buffer the proton layer from the Rayleigh-Taylor-like (RT) instability that would have otherwise degraded the proton beam acceleration. A simple three-interface model is formulated to qualitatively explain the stabilization of the light-ions acceleration. Due to the absence of the RT-like instability, the produced high quality mono-energetic proton bunch can be well maintained even after the laser-foil interaction concludes.

PACS numbers: 52.40.Nk, 52.35.Mw, 52.57.Jm, 52.65.Rr

In the past decades, plasma-based ion accelerators have attracted a lot of attention due to their potential applications for particle acceleration, medical therapy [1], proton imaging, and inertial confinement fusion (ICF) [2]. One of the most important issues is the development of laser-driven protons for radiation therapy of deep-seated tumours [3]. Numerous experimental and theoretical studies have been devoted to producing such proton beams [4–6]. However, their qualities such as beam collimation, energy spread ( $\sim 20\%$ ), and peak energy ( $\sim 58$  MeV), are still unsatisfactory [5].

Recently, with the rapid development of the laser technology, ultraintense ultrashort ultraclean (3U) laser pulse and ultrathin solid target have been extensively exploited to investigate the ion acceleration. One of the most straightforward acceleration mechanisms, radiation pressure acceleration (RPA) [6], is being revisited. The first RPA experiment [7] has shown that both the beam quality and the energy conversion efficiency are greatly improved. However, the ultrathin foil is very susceptible to the transverse instabilities [8], similar to Rayleigh-Taylor-like (RT) instability in ICF. It sets in at the very beginning of laser-foil interaction and develops at the unstable interface at the rate of a few laser cycles [9]. Gradually, the surface of the foil becomes corrugated by the laser radiation and the entire target is torn into many clumps and bubbles [8]. The final energy spectrum of the ions shows a quasi-exponential decay with sharp cut-off energy. Unlike the electron acceleration in the bubble regime [10], a stable proton beam acceleration in the realistic three-dimensional (3D) geometry has not been demonstrated either theoretically or experimentally.

In this Letter, we report on a new regime of stable proton acceleration, where a two-specie ultra-thin shaped foil is illuminated by a circularly polarized (CP) laser pulse. We assume the heavier (lighter) ions to be carbons (protons), respectively. Particle-in-cell (PIC) simulations indicate that the RT instability only causes the spreading of the carbon ions. The protons, which are rapidly separated from the carbon ions, are "buffered" by the carbon ion cloud by riding on the stable proton-carbon interface. We demonstrate that, even though the RT-unstable carbon-vacuum interface is strongly deformed, the feed-through of the RT instability into the RT-stable proton-carbon interface is small. Due to the absence of the RT instability, the compact proton layer remains well-collimated even after the laser-foil interaction concludes. In order to elucidate the detailed acceleration process, we first describe the results of 1D simulations. Discussion of the influence of the RT instability on the ion acceleration follows, backed up by 3D simulations.

When a relativistic laser pulse illuminates a two-specie foil with thickness of a few wavelengths, a collisionless shock wave is often excited and can efficiently accelerate the ions to high energies [11]. With the decreasing foil thickness, the laser radiation pressure competes with the shock wave and becomes strong enough to push the entire foil forward. As a result, the foil acceleration is dominated by the RPA. The critical foil thickness can be approximately estimated by [12]

$$L \sim \frac{a}{\pi} \frac{n_c}{n_e} \lambda, \quad (1)$$

where  $a = eE_L/m_e c \omega$  is the dimensionless laser amplitude,  $m_e$  the electron mass,  $n_e$  the electron density, and  $n_c$  is the critical plasma density.  $c$ ,  $\omega$ ,  $\lambda$ , and  $E_L$  are the light speed in vacuum, the laser frequency, wavelength and electric field, respectively. In the 1D RPA model, the target motion equation is governed by

$$\rho \frac{d(\gamma\beta)}{dt} = \frac{E_L^2}{2\pi c} \frac{1-\beta}{1+\beta}, \quad (2)$$

where  $\rho = \sum_i m_i n_i L$  is the target area mass density,  $m_i$  and  $n_i$  are the ion mass and density,  $\beta = v/c$  is the target velocity and  $\gamma = 1/\sqrt{1-\beta^2}$  is the relativistic factor. We can see that the target dynamics is defined by the area density, not the detailed foil composition. In principle, the heavier ions can be efficiently accelerated to the same velocity as the lighter protons and electrons.

We simulate the described mechanism using the PIC code VLPL [13]. The longitudinal length of the 1D simulation box is  $x = 60\lambda$  sampled by  $6 \times 10^4$  cells, enough to resolve the expected density spikes. Each cell contains 100 numerical macro particles in the plasma region. The target is  $0.1\lambda$  thick, located at  $x = 10\lambda$  and composed of carbon ions and protons with the same number density  $46.7n_c$ , which gives the electron density  $n_e = 320n_c$ . A CP laser pulse with the wavelength  $\lambda = 1.06\mu m$  is incident on the target from the left boundary. The wave front of the laser arrives at the target surface at  $t = 10T_0$ , where  $T_0 = \lambda/c$  is the laser cycle. The laser pulse is homogeneous in space but has a trapezoidal profile (linear growth - plateau - linear decrease) in time. The duration is  $\tau_L = 10T_0$  ( $1T_0 - 8T_0 - 1T_0$ ). The dimensionless laser amplitude  $a = 100$  is chosen to satisfy Eq. (1).

Figure 1(a) shows the particle density distribution at  $t = 20T_0$ . In the initial stage, the laser pressure is transferred to the electrons, resulting in the charge separation [12]. Because

carbons and protons are initially co-located, the protons experience a higher acceleration due to their higher charge to mass ratio ( $Z_i/m_i$ ). The time for protons to separate from the carbon ions is approximately  $t_{sep} = \sqrt{2Lm_H/eE_L} = 2.5fs$ , which is so short that can be considered instantaneous. Later on, the two ion species start experiencing very different acceleration field, as shown by the red curve in Fig. 1(a). The considerably higher electric field inside the carbon layer compensates for carbon's lower  $Z_i/m_i$  ratio enabling them to catch up with the protons. Eventually, both species travel together, without separating any further. The entire foil acceleration proceeds until the end of the laser-foil interaction at  $t = 35T_0$ . Fig. 1(b) exhibits the phase space distribution. We can see that the carbon ions fall back behind the protons, accompanied by a long low-density tail. The fact that both ions show an obvious "spiral structure" [14] in phase space provides a direct evidence for the acceleration process described above.

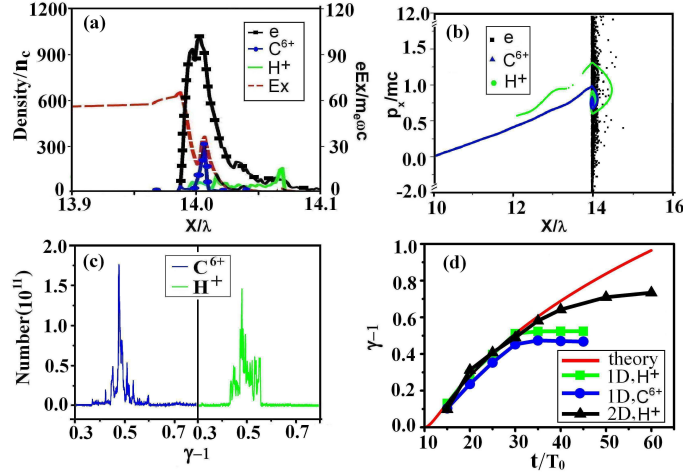


Figure 1. (Color online). (a) Density distribution of the electrons (black), protons (green), and carbon ions (blue) at  $t = 20T_0$ . The red curve shows the electric field  $E_x$ , which is normalized to  $E_0 = m_e c \omega / e = 3.2 \times 10^{12} \text{V/m}$ . (b) The corresponding phase space distribution at  $t = 20T_0$ . (c) Energy spectrum of the carbon ions (blue, dark) and protons (green, light) at  $t = 30T_0$ . (d) Energy evolution in time from PIC simulations and the 1D theory. The laser pulse is incident from the left side and touches the foil at  $t = 10T_0$ .

The ion energy spectrum is shown in Fig. 1(c). At  $t = 30T_0$ , the peak energy of the carbon ions is up to 480MeV/u. For protons, all of them are accelerated to high energies although the energy spectrum is somewhat wider. Fig. 1(d) plots the ion energy evolution.

Here, we make use of the averaged energy for both species. At  $t = 35T_0$ , the laser-foil interaction is over so that the ion energy doesn't increase any more. Overall, the observed ion acceleration in the 1D simulations is consistent with the predictions of the 1D theory of Ref. [12].

However, multi-dimensional simulations exhibit a radically different acceleration dynamics because multi-dimensional effects - such as transverse expansion of the bunch and the RT instability - come into play. In order to extend the 1D model to the 2D simulations smoothly, we employ a shaped foil target (SFT) [15] to compensate for the transverse profile of the laser pulse. Taking the Gaussian laser for example, the foil thickness should be matched transversely by the Gaussian function  $L = \max[L_{\max} \exp(-y^2/\sigma_T^2), L_{\text{cut}}]$ , where  $L_{\max}$  is the maximal foil thickness,  $L_{\text{cut}}$  the cutoff thickness, and  $\sigma_T$  the spot radius. In the following 2D case, the simulation box is  $X \times Y = 80\lambda \times 32\lambda$ , sampled by  $16000 \times 400$  cells. Each cell contains 100 macro particles in the plasma region. The foil is initially located at  $x = 10\lambda$  with parameters  $L_{\max} = 0.1\lambda$ ,  $L_{\text{cut}} = 0.05\lambda$ , and  $\sigma_T = 7\lambda$ . The carbon ion density is  $51.9n_c$ , intermingled with protons of the density  $8.64n_c$  so that the total electron density is  $320n_c$ . A Gaussian laser pulse with the focal size  $\sigma_L = 8\lambda$  is incident from the left boundary. All other parameters are the same as in the 1D case.

Fig. 2(a) shows the space distribution of the carbon ions and protons at different times. In each frame, the cyan color marks the carbon ions and the red color shows the protons. Obviously, the carbon ions behave totally different as compared with the 1D simulations. They spread widely in space and do not form a compact mono-energetic bunch. On the contrary, the protons from the center part of the foil always ride on the carbon ion front and form a compact bunch. The sharp front separating the species is well defined and remains stable even after the laser-foil interaction concludes. We can get further understanding of the acceleration process from the phase space distribution in Fig. 3 (a) and (b). On the one hand, the carbon ions evolve into a wide cloud in space. On the other hand, their front co-moves with the fast protons so that the gap between the two species is always small. The protons show a clear spiral structure, like a "matchstick", which coincides with the 1D simulation result in Fig. 1(b). We don't observe any obvious transverse instability in the compact proton layer. Fig. 2(b) shows the proton energy spectrum. As expected, the peak is well pronounced and the dispersion is suppressed. The peak energy evolution is presented in Fig. 1(d), which is also in accordance with the 1D RPA model. Fig. 3(c, d) plots the ion

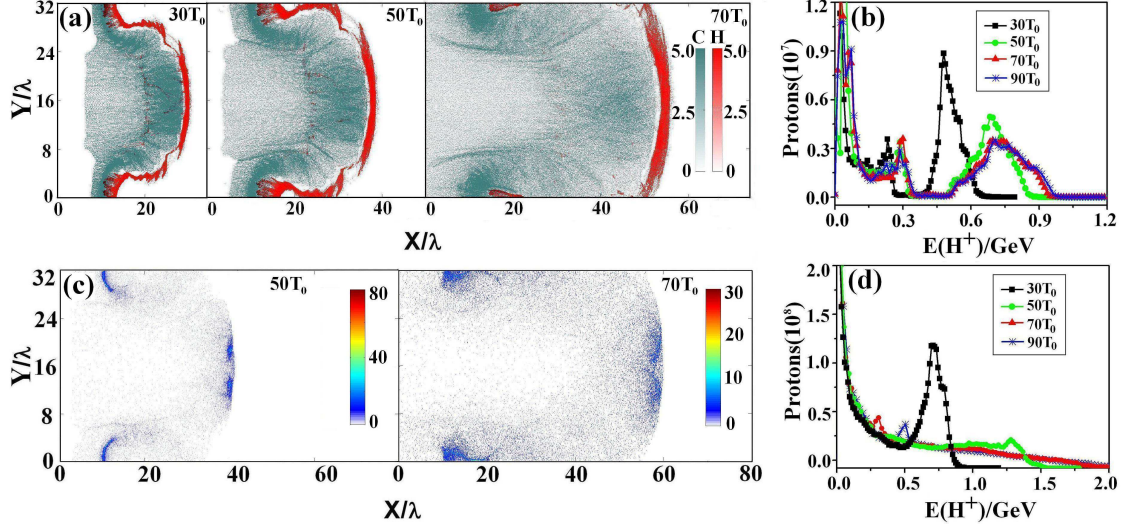


Figure 2. (Color online). (a) Contours of protons (red, dark) and carbon ions (cyan, light) in the 2D case at different time points:  $t = 30T_0, 50T_0$ , and  $70T_0$ . The colorbar represents the proton numbers  $\log(N)$ . (b) Proton energy spectrum at:  $t = 30T_0$  (square, black),  $t = 50T_0$  (circle, green),  $t = 70T_0$  (triangle, red), and  $t = 90T_0$  (star, blue). For comparison, Frame (c) shows the proton density distribution in a pure Hydrogen foil and Frame (d) corresponds to its energy spectrum evolution.

energy-divergency distribution at  $t = 30T_0$ . The high quality proton bunch with the energy  $\sim 500\text{MeV}$  and the opening angle  $\sim 5.5^\circ$  forms and persists in time even after the laser-foil interaction concludes.

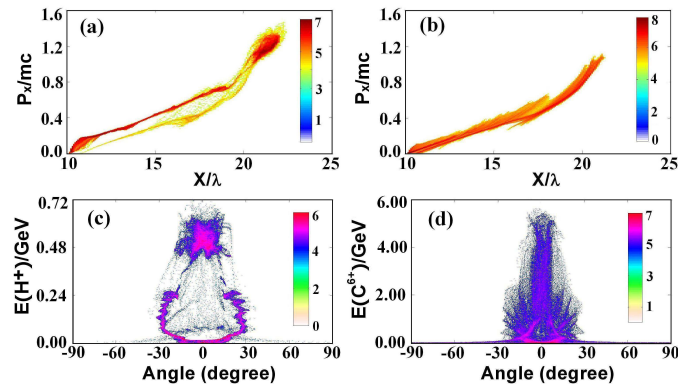


Figure 3. (Color online). Phase space of (a) protons and (b) carbon ions at  $t = 30T_0$ . An obvious spiral structure is observed only for protons. Frame (c) and (d) show the carbon ion and proton energy distribution as a function of the divergency angle at  $t = 30T_0$ .

The stability of the proton acceleration in the 2D simulations can be attributed to two effects. Firstly, the protons completely separate from the carbon ions and form a thin shell, which is a prerequisite for the stable proton acceleration. Such a separation of the ion species can be understood within the 1D formalism developed in Ref. [12] and the 1D simulation above. Secondly, the heating of the carbon ions forms an extended cloud that prevents short-wavelength perturbations from feeding through into the thin proton shell. We can use a simple three-interface model as shown in Fig. 4 to explain the stabilization. It is helpful to consider the problem from the classical RT instability [16] which occurs when a light fluid is accelerated into a heavy fluid. In the accelerating reference frame of the foil, the perturbation pressure  $p$  satisfies:

$$\frac{\partial^2}{\partial z^2} \delta p = -k_{\text{RT}}^2 \delta p, \quad (3)$$

where  $k_{\text{RT}}$  is the wavenumber of the RT-unstable mode. Noting that  $\delta p$  is discontinuous across the unperturbed boundary, we obtain a solution  $\delta p = A_i e^{-k_{\text{RT}} z} + B_i e^{k_{\text{RT}} z}$  away from interfaces, with  $A_i$  and  $B_i$  being the amplitude coefficients of the perturbation inside the layer consisting of the  $i$ 'th species. In our case, both species have two interfaces: one with vacuum and one with the other specie. For carbon ions ( $i = C$ ), the only unstable interface is the carbon-vacuum boundary, where the laser pulse interacts directly with the carbon plasma. We derive from this model that the amplitude of the RT instability is exponentially decaying away from the unstable interface:

$$\frac{A_H}{A_C} \sim e^{-k_{\text{RT}} L_C}, \quad (4)$$

where  $L_C$  is the thickness of the carbon ion layer. In the simulations,  $L_C$  is several times longer than  $L_H$  so that the long-wavelength perturbation in the carbon layer would take much more time to grow (recall that the growth rate of the RT instability  $\gamma \propto \sqrt{g/\lambda_{\text{RT}}}$ , where  $g$  is the target's acceleration and  $\lambda_{\text{RT}}$  is the perturbation wavelength). The feed-through from the unstable carbon-vacuum interface to the proton layer is exponentially attenuated according to Eq. (4). This simple qualitative argument explains the stability of the sharp carbon-proton interface. For the thin proton layer, it is also stable because the protons are much lighter than the carbon ions. Eventually, the entire proton layer is free from the RT instability. Besides, we believe that the small transverse size of the foil also

benefits the stabilization of the proton acceleration in this case. Approximately, the minimal perturbation wavenumber can be estimated by  $k_{RT} = 2\pi/Y$ , where  $Y$  is the transverse foil size. At  $t = 30T_0$ , the carbon shell thickness is  $L_C \approx 10\lambda$  and  $Y = 32\lambda$ . Eq. (4) already indicates a considerable suppression of the perturbation feed-through.

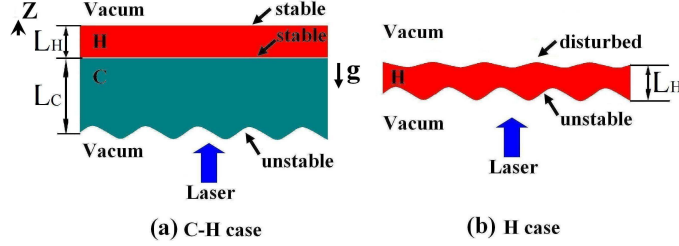


Figure 4. (Color online). Schematic of laser-foil interaction in (a) C-H case and (b) pure H case. The red color marks the protons and the cyan represents the carbons. In case (a), there are three interfaces: carbon-vacuum, carbon-proton, and proton-vacuum. Only the first interface is unstable. In case (b), both interfaces are finally unstable.

Now we compare the stable multi-component foil case with the pure proton foil case, where the RT instability is obvious. We again employ a matched SFT. All the parameters are the same as above except now  $n_H = 320n_c$  and the carbon ions are absent. Fig. 2(c) shows the proton density distribution in space. We can see that the foil disrupts gradually and two proton bunches with a lower density valley in the middle form. This is very characteristic for the RT instability driven by the laser radiation. According to the linear stability theory for the accelerated foil [8], the growth time of the perturbation in the relativistic limit can be derived as following

$$\frac{\tau_{RT}}{T_0} = \frac{\sqrt{2}}{6} \sqrt{\frac{m_e n_c \lambda}{m_i n_i L}} \left( \frac{\lambda_{RT}}{\lambda} \right)^{3/2} a, \quad (5)$$

Taking into account  $\lambda_{RT} \simeq \sigma_L = 8\lambda$  and  $L = 0.1\lambda$  in our case, we estimate that the time scale of the instability should be  $2.2T_0$ . Such a short-wavelength perturbation grows very fast so that it reaches the other side of the foil soon. Finally, both interfaces are unstable and the entire target collapses quickly. Fig. 2(d) shows the proton energy spectrum. Although an energy peak is observed initially, it lowers gradually and disappears at  $t = 45T_0$ , leaving a quasi-exponential spectrum. In fact, most single-ion foils in the RPA regime show a similar simulation result [6, 8, 14, 15]. The main issue is the fast growth of the short-wavelength



perturbation at the unstable interface.

In order to check the robustness of the stable regime, we perform 3D simulations while keeping all the parameters same as in the 2D case except  $\sigma_T = 6\lambda$ . A stable structure of the proton beam acceleration is also observed, which indicates that the regime described above can significantly stabilize the proton beam acceleration in the realistic three dimensional geometry.

In conclusion, we present a new regime of stable proton acceleration driven by the laser radiation. In this regime, we smoothly extend the 1D RPA model to multi-dimensional cases by using a two-specie ultra-thin SFT. PIC simulations show that the transverse instability degrades only the carbon ion acceleration and spreads them in space. The sharp front separating the species is always stable so that the proton layer is free from the effects of the RT instability. Benefiting from the superpower lasers such as HiPER and ELI, this stable regime might open a way to high quality proton beam generation in the future.

We thank the fruitful discussions with F. Q. Shao, N. Kumar, and Y. Y. Ma. This work is supported by the DFG programs GRK1203 and TR18. TPY thanks the scholarship awarded by China Scholarship Council (CSC NO. 2008611025) and the NSAF program (Grant No. 10976031).

---

\* Electronic mail: pukhov@tp1.uni-duesseldorf.de

- [1] S. V. Bulanov, *et al.*, Phys. Lett. A **299**, 240 (2002).
- [2] T. Ditmire, *et al.*, Nature (London) **398**, 489 (1999).
- [3] A. R. Smith, Med. Phys. **36**, 556 (2009).
- [4] B. M. Hegelich, *et al.*, Nature (London) **439**, 441 (2006); D. Neely, *et al.*, Appl. Phys. Lett. **89**, 021502 (2006); L. Willingale, *et al.*, Phys. Rev. Lett. **96**, 245002 (2006); Y. Y. Ma, *et al.*, Phys. Plasma **16**, 034502 (2009); T. P. Yu, *et al.*, Phys. Plasma **16**, 033112 (2009).
- [5] H. Schworer, *et al.*, Nature (London) **439**, 445 (2006).
- [6] A. P. L. Robinson, *et al.*, NEW J. Phys. **10**, 013021 (2008); A. Macchi, *et al.*, Phys. Rev. Lett. **103**, 085003 (2009); B. Qiao, *et al.*, Phys. Rev. Lett. **102**, 145002 (2009); M. Chen, *et al.*, NEW J. Phys. **12**, 045004 (2010); S. V. Bulanov, *et al.*, Phys. Rev. Lett. **104**, 135003 (2010).
- [7] A. Henig, *et al.*, Phys. Rev. Lett. **103**, 245003 (2009).

- [8] F. Pegoraro, and S. V. Bulanov, Phys. Rev. Lett. **99**, 065002 (2007); X. Q. Yan, *et al.*, Phys. Rev. Lett. **103**, 135001 (2009); S. V. Bulanov, *et al.*, Eur. Phys. J. D **55**, 483-507 (2009).
- [9] M. Chen, *et al.*, Phys. Plasmas **14**, 113106 (2007).
- [10] A. Pukhov and J. Meyer-ter-Vehn, Appl. Phys. B **74**, 355 (2002).
- [11] L. Ji, *et al.*, Phys. Rev. Lett. **101**, 164802 (2008); X. Zhang, *et al.*, Phys. Rev. Special Top.-Accel.Beams **12** 021301 (2009).
- [12] V. K. Tripathi, *et al.*, Plasma Phys. Control. Fusion **51**, 024014 (2009).
- [13] A. Pukhov, J. Plasma Phys. **61**, 425 (1999).
- [14] A. Macchi, *et al.*, Phys. Rev. Lett. **94**, 165003 (2005); X. Q. Yan, *et al.*, Phys. Rev. Lett. **100**, 135003 (2008).
- [15] M. Chen, *et al.*, Phys. Rev. Lett. **103**, 024801 (2009); T. P. Yu, *et al.*, Laser Part. Beams **27**, 611-617 (2009).
- [16] L. Rayleigh, Proc. London Math. Soc. **14**, 170 (1882); G. I. Taylor, Proc. R. Soc. A **201**, 192 (1950).